*J. Electrochem. Sci. Eng.***13(6)** (2023) 1037-1050; http://dx.doi.org/10.5599/jese.1951

Open Access : : ISSN 1847-9286
www.jESE-online.org

Original scientific paper

Electrochemical and optical studies on photoactive $BiVO_4$-TiO_2/ /poly 3,4-ethylenedioxythiophene assemblies in gel electrolyte: Role of inorganic/organic interfaces in surface functionalization

Kasem K. Kasem✉, Mattie Tom, Mehreen Tahir and Logan Cox

School of Sciences, Indiana University Kokomo, Kokomo, IN, 46904, USA

Corresponding author: ✉kkasem@iuk.edu

Received: June 26, 2023; Accepted: September 2, 2023; Published: September 19, 2023

Abstract

Inorganic/organic interface assemblies were created from poly 3,4-ethylenedioxythiophene (PEDOT) interfaced with amorphous $BiVO_4$ and with $BiVO_4$-TiO_2. Electrochemical cells-based thermoplastic gel electrolytes containing KI/I_2 were used to study the photoelectrochemical behavior of the Inorganic/organic interface electrodes. Optical studies show that doping $BiVO_4$ with TiO_2 narrowed the optical band gap to allow more absorption in the visible region and increases solar energy conversion. Evidence for both direct and indirect band gaps was observed. Refractive index data indicates that $BiVO_4$ and $BiVO_4/TiO_2$ obey the anomalous dispassion multiple-oscillator model. Chronoamperometry of these assemblies shows the phenomena of dark current, which correlates to the presence of random electron/hole generation in the depletion layer. PEDOT enhances the photoactivity of $BiVO_4$ only. Electrochemical impedance spectroscopy studies indicated that both kinetic and diffusional control at high and low frequencies, respectively. Furthermore, studies show that as frequency increases, the conductivity increases due to dispersion and charge carrier hopping. All photoactivity outcomes were reproducible.

Keywords

Photoelectrochemistry, organic semiconductor polymer, gel electrolytes, metal oxides/organic interfaces

Introduction

Effective photoactive materials possess a narrow bandgap for visible light activities, noticeable electron-hole separation, longer electron lifetime, and longer charge carrier diffusion length. Among these materials are transition metal oxides, which possess several functional properties. Their crystal structure, composition, intrinsic defects, and doping may determine their optical, dielectric, and catalytic outcomes. To have the desired band gaps and conduction band (CB) edge positions that can be used in a needed photoelectrochemical process, a selective method of preparation must

be used. The process's parameters strongly govern the morpho-structural characteristics and, therefore, the physicochemical properties of metal oxides [1,2].

Bandgap modulation, microstructure, and optoelectronic properties are fundamental for a wide range of metal oxide applications [3-6]. Several studies were performed with some transition metal oxides, such as WO_3 as a planar electrochemical sensor [3] and as a sensor for NO_2 [4]. Studies were carried out on ZnO [5,6], TiO_2 [7], Fe_2O_3[8], and Co_3O_4 [9] to name but a few.

The photochemical stability of TiO_2 drove the attention to couple it with another metal oxide to create narrower band gap assemblies. Examples of such work includes NiO/TiO_2 [10], Ag_2O/TiO_2 [11], Bi_2O_3/TiO_2 [12], SnO_2/TiO_2 [13], Fe_2O_3/TiO_2 [14]. Narrow or small band gap semiconductors increase the absorption of visible light. It also inhibits photo-generated electron-hole recombination in a semiconductor heterojunction structure. To overcome the intrinsic limitations of binary metal oxides, several studies were directed to investigate the use of multiple cations to build multi-ternary oxides. These multi-ternary oxide assemblies, which contain some post-transition metal elements, should possess band gap edges that can be aligned with some desired redox systems. Mixed-valence transition-metal oxides with a spinal structure were found to be catalytically active for oxygen reduction reactions in alkaline conditions [15]. Further, the catalytic activities of $Bi_{20}TO_{32}$ [16], $SnNb_2O_6$ [17], and $BiVO_4$ [18,19] with visible light were investigated. Some studies show that the overall performance of $BiVO_4$ is limited by poor carrier transport properties [20,21]. Such poor carrier transport lengths were explained on the basis that some doping strongly decreases carrier mobility by introducing intermediate-depth donor defects as carrier traps [22].

Most studies on $BiVO_4$ took place in liquid electrolytes to investigate its effectiveness in water splitting to produce hydrogen and oxygen. Recently, $BiVO_4$ has been used as a competitive anode in lithium-ion batteries [23,24]. Some metal oxide composites in connection with reduced graphene (rGO) or other conducting polymers in what is known as pseudocapacitors have been studied [25-27].

The lack of studies on the photoelectron-chemical (PEC) behavior of $BiVO_4$ in gel electrolytes or under immobilization conditions drove our interest in exploring the PEC behavior of pure $BiVO_4$ and $BiVO_4$-TiO_2 /poly 3,4- ethylene-dioxythiophene (PEDOT) interfaces in thermoplastic gel electrolyte (TPGE). The objective is to study the contribution of the $BiVO_4$ /PEDOT interface to the PEC outcome in TPGE. One of the advantages of gel electrolytes is their potential to the creation of safe electrochemical (EC) devices (batteries or supercapacitors). Both $BiVO_4$, and PEDOT are electrochemically stable, and TPGE has no hazardous effect. Our goal is to have a stable and reproducible electrochemical system that provides useful data for future applications.

Experimental

Reagents

The monomer 3,4-ethylenedioxythiophene (EDOT) (Alfa Aesar Inc., USA) was used to prepare poly 3,4-ethylenedioxythiophene (PEDOT). All other chemicals used were of analytical grade. Unless otherwise stated, all the solutions were prepared using the appropriate solvents, and deionized (DI) water was used for the aqueous solution.

Preparations

Both $BiVO_4$ and $BiVO_4$-TiO_2 were prepared as previously described [19], briefly, $BiVO_4$ and/or $BiVO_4/TiO_2$ composites are synthesized by adopting a sol-gel method and a facile hydrothermal route. A Teflon-lined stainless steel autoclave of 100 mL capacity was used and maintained at 190 °C for 8 h to get the needed composite. The obtained products were collected by centrifugation and

washed several times with deionized water and dried at 90 °C for 12 h. Suspensions of $BiVO_4$ or $BiVO_4$-TiO_2 in acetonitrile were dispersed evenly on the surfaces of fluorinated tin oxide (FTO) to create FTO/$BiVO_4$ and FTO/$BiVO_4$-TiO_2 and allowed to dry at 40 °C. at ambient conditions for 4 hours. The inorganic/organic interface (IOI) thin films of $BiVO_4$ and $BiVO_4$-TiO_2 deposited on FTO occluded in PEDOT were prepared electrochemically, using cyclic voltammetry (CV) technique, by repetitive cycling (3 cycles) of the FTO glass electrode potential between -0.5 V and 1.7 V *vs*. Ag/AgCl in an acetonitrile suspension (1 mg/mL) of the inorganic materials, 5 mM of the EDOT monomer and 0.2 M $LiClO_4$.

Preparation of thermoplastic gel electrolyte (TPGE)

Thermoplastic gel electrolyte (TPGE) was prepared following the published procedure [28]. Briefly, 0.65M KI and 0.065M I_2 were dissolved in 10 mL polycarbonate (PC), and then 8.5 g of PEG (M-20 000) was added to the mixture. The mixture was heated at 100 °C under continuous stirring for *ca.* 12 h in a flask under an inert atmosphere. The mixture was hydrothermally treated at 180 °C for 14 h in a Teflon autoclave container.

Instrumentation

A conventional three-electrode cell consisting of a Pt sheet as a counter electrode, an Ag/AgCl reference electrode, and FTO with a surface area of 2.0 cm^2 was used as the working electrode for occlusion electrodeposition of $BiVO_4$ or $BiVO_4$-TiO_2 during electrochemical polymerization of EDOT. Photoelectrochemical studies of the thin solid films in gel electrolyte were performed using the experimental setup described in Figure 1, where the FTO covered with the photoactive material was a working electrode and platinized FTO (Pt-FTO) served as both reference and counter electrode. The gel electrolyte was poured on top of the working electrode, and the counter electrode was pressed on top of the gel electrolyte to make a uniform electrolyte thickness of 10 µm (Figure 1). A Solartron 2101A, USA, was used for the electrochemical impedance spectroscopy (EIS) studies in a frequency range between 100 kHz to 0.01 Hz. A BAS 100W electrochemical analyzer (Bioanalytical Co. IN, USA) was used to perform electrochemical studies. Optical parameters were calculated based on the steady-state reflectance spectra measured by the Shimadzu UV-2101PC spectrophotometer. Irradiations were performed with a solar simulator 300-watt xenon lamp (Newport, NJ, USA) with an IR filter. All measurements were performed at 298 K.

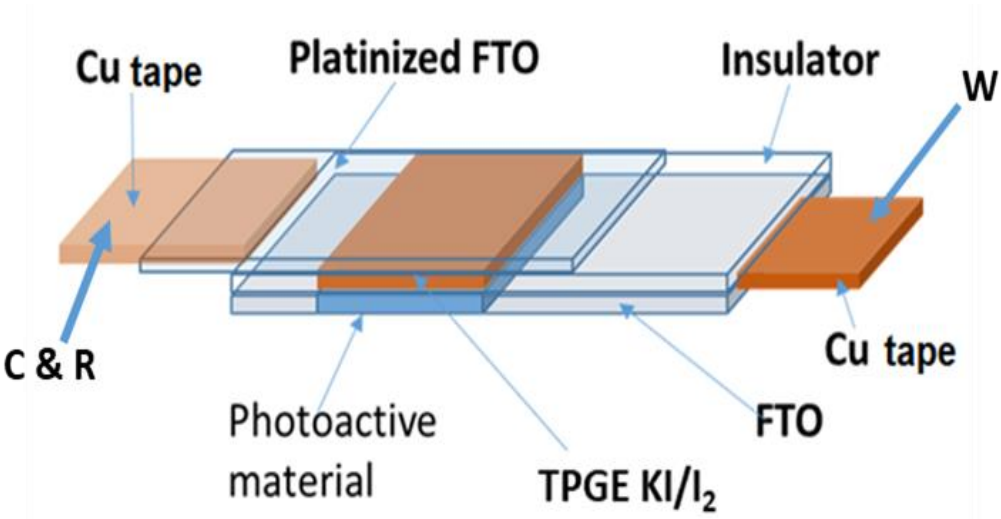

Figure 1. *Electrochemical cell-based thermoplastic gel electrolyte setup. W = working electrode, C = counter electrode, R = reference electrode*

Results and discussion

Optical studies

Optical bandgap

The absorption spectra of $BiVO_4$ and $BiVO_4$-TiO_2 were investigated along with other optical parameters such as refractive index (n) and optical conductivity (σ_{opt}). Both n and σ_{opt} have been calculated and plotted as a function of photon energy, the results are displayed in Figures 2, 3, and 4. Figure 2 A indicates that doping $BiVO_4$ with TiO_2 narrowed the band gap to allow absorption in the visible region. This behavior is related to the formation of surface states at the interface of $BiVO_4$-TiO_2 heterojunction, as it was also reported in other composite materials such as ZrO_2/TiO_2, SnO_2/TiO_2 and WO_3/$BiVO_4$ [13]. Furthermore, Figures 2B and 2C were obtained after treatment of the absorption data in Figure 2A, as plots of $\alpha^{½}$ *vs.* photon energy [hv] and $(\alpha hv)^2$ *vs.* hv respectively, where α is the absorption coefficient as described in previous studies [29]. Figures 2B and 2C indicate the existence of both direct and indirect band gaps in the studies assemblies. The estimated values of these band gaps are listed in Table 1. While the absorption spectrum for PEDOT is not displayed, the bandgap, direct, and indirect bandgap values are listed for comparison. The existence of direct or indirect bandgaps may indicate the creation of interfacial hybrid sub-bands with the PEDOT interface. This also indicates that doping $BiVO_4$ with TiO_2 shifts the absorption peak to photon energies smaller than the undoped $BiVO_4$.

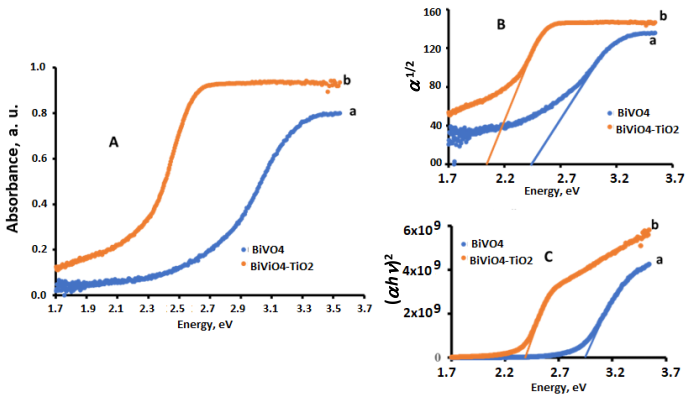

Figure 2. *A) Absorption spectra, B) plots of $\alpha^{½}$ vs. hv, and C) $(\alpha hv)^2$ vs. hv*

The contribution of the hard/soft acid-base characteristics (HSAB) to the reactivities of these composites on FTO can be evaluated from a calculation of ΔN (the fraction of electrons transferred between the assemblies and the FTO interface) [30]. The calculated hardness (η), electronegativity (χ), softness ($š$), and ΔN are listed in Table 1. The calculated η of $BiVO_4$-TiO_2 is less than that of $BiVO_4$, while that of PEDOT is the least. Thus, $š$ increases in this order PEDOT> $BiVO_4$-TiO_2> $BiVO_4$. Such an increase in the acid softness character reflects strong adsorption on the substrate. Such adsorption facilitates the electron transfer process. The values of ΔN listed in the table are calculated as published elsewhere [30], indicating the fraction of electron transfer between the substrate (FTO glass) and any studied composites. The increase of ΔN is evidence of increasing electron transfer at the thiophene-substrate interface.

Table 1. *The optical band gap and other acids/base characters for the studied compounds*

Assembly	χ	Direct band gap, eV	Electron affinity, eV	Ionization potential, V	η / eV	$\check{s}$ / eV^{-1}	ΔN
$BiVO_4$	6.04	2.90	4.56	7.46	1.45	0.689	1.48
$BiVO_4$-TiO_2	5.92	2.40	4.86	7.26	1.20	0.833	1.59
PEDOT	3.38	2.15	2.3	4.45	1.07	0.933	1.20
FTO	3.35	3.45	1.65	5.1	1.73	0.578	

Refractive index

The optical, electronic, and optoelectronics properties of a semiconductor (SC) material are dictated by its refractive index (n) and its energy gap (E_g). The refractive index is a measure of the SC transparency to the incident spectral radiation [31]. The greater the polarizability of the interface the greater the n. On that basis, the refractive index can reflect the purity of the system and the coexistence of multiple phases. The greater the deviation of n from the accepted measured value for a pure substance, the greater the existence of multiple phases.

Equations (1) and (2) [32,33] are based on the general assumption that all energy is scaled down by $1/\varepsilon_{eff}$, where ε_{eff} is the dielectric constant.

$$n^4/\lambda = 0.077/nm^{-1} \quad (1)$$

$$n^4 E_g = 95 \quad (2)$$

where λ is the wavelength, nm. The plot of refractive index (n) *vs.* photon energy is displayed in Figure 3. The wavelength corresponding to the absorption edge is 450 nm for $BiVO_4$ and 550 nm for $BiVO_4$-TiO_2. According to Equation 1, the calculated n value for $BiVO_4$ is 2.43, while n for $BiVO_4$-TiO_2 is ≈2.55. Figure 3 indicates that these n values correspond to an E_g of 2.0 eV for $BiVO_4$-TiO_2 and E_g ≈2.6 eV for $BiVO_4$. These E_g values support the presence of an indirect bang gap (*cf.* Figure 2B). This validates the approximation of Equation 2, as applying the indirect E_g values in this equation generates n = 2.47 for $BiVO_4$ and n = 2.46 for $BiVO_4$-TiO_2. These values agree with previous studies [34]. Figure 3 also indicates that the refractive index increases with increasing photon energy (shorter λ) and decreases at low photon energy (longer λ). High n means that light travel through the sample is slow. Such slow light travel will result in changing light direction and other optical properties related to this change. The material with a high n is designated as optically denser. Doping $BiVO_4$ with TiO_2 lowers the band gap and increases the refractive index.

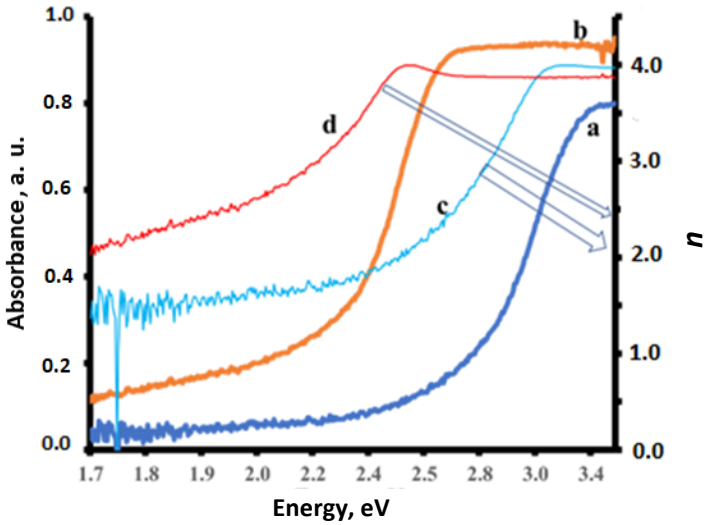

Figure 3. *The absorbance of (a) $BiVO_4$, and b) $BIVO_4$-TiO_2, and refractive index n vs. photon energy of (c) $BiVO_4$, and d) $BIVO_4$-TiO_2*

Optical conductivity σ_{opt} and electrical conductivity σ_{ele}

Both σ_{opt} and σ_{ele} were calculated using equations (3) and (4) [35,36]:

$$\sigma_{opt} = \frac{\alpha n c}{4\Pi} \quad (3)$$

$$\sigma_{ele} = \frac{2\lambda\sigma_{opt}}{\alpha} \quad (4)$$

Figure 4 clearly shows that 1) σ_{opt} increases with increasing photon energy up to 2.4 eV for $BIVO_4$-TiO_2, while σ_{opt} for $BiVO_4$, increases up to 3.4 eV, after which they remain constant for both compounds: 2) $BIVO_4$-TiO_2 has a greater conductivity than $BiVO_4$ and 3) the great rise around the band gap of each assembly can be attributed to the electron excitation in this range of photon energy. Figure 4 also indicates that optical conductivity is much greater than electrical conductivity. Such behavior can be explained based on the Edwards [37] or the Drude model [38]. However, electrical conductivity for $BiVO_4$ increases with increasing photon energy, while that of $BIVO_4$-TiO_2 reaches a maximum at photon energy ca 2.4 eV and then decreases with increasing photon energy.

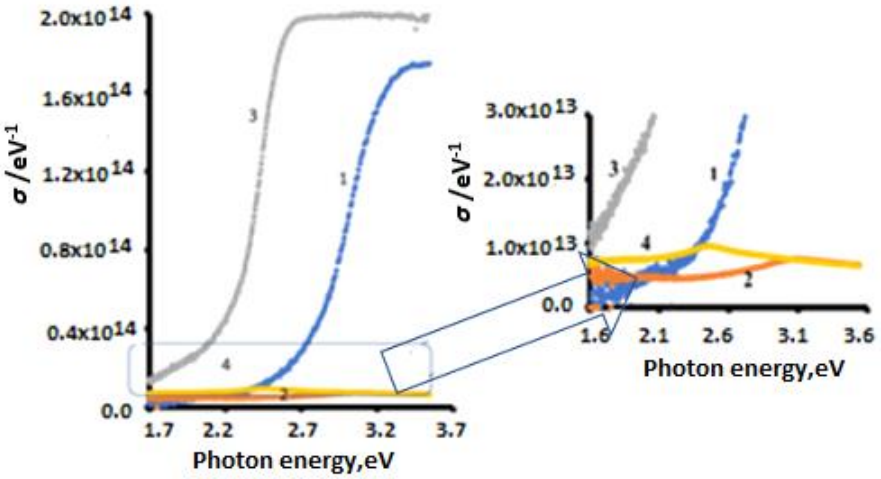

Figure 4. *Optical conductivity* vs. *photon energy of 1) $BiVO_4$ and 3) $BiVO_4$-TiO_2; and electrical conductivity (σ_{ele}) of 2) $BiVO_4$, and 4) $BiVO_4$-TiO_2*

Photoelectrochemical (PEC) behavior

All electrochemical studies performed in gel electrolyte took place in the electrochemical cell described in Figure 1, where the modified FTO with either inorganic or organic PEDOT both acts as working electrode, thermoplastic KI/I_3^- gel acts as an electrolyte, and platinized FTO (Pt/FTO) acts as both counter and reference electrode.

Effect of TiO_2 on the EC behavior of $BiVO_4$ thin film

PEC studies were performed in the dark and under illumination, with a scan rate of 0.10 V s^{-1}, between -1.5 to 2.0 V unless otherwise stated. The results are displayed in Figure 5. This figure shows that upon illumination, an increase in the photocurrent for FTO/$BiVO_4$ (trace 3 or FTO/$BiVO_4$-TiO_2 (trace 4) in both cathodic and anodic scans. Furthermore, FTO/$BiVO_4$-TiO_2 gives the highest photocurrent, which indicates that TiO_2 enhances the charge separation and decreases the (e/h) recombination. This is consistent with the values of ΔN (listed in Table 1), as $BiVO_4$-TiO_2 has greater ΔN than $BiVO_4$.

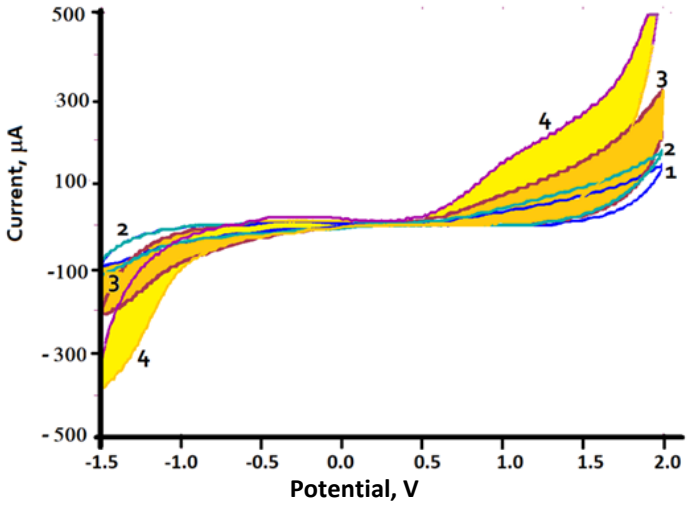

Figure 5. *I / µA and E / V at scan rate 0.1 V s^{-1} for metal oxides/FTO in gel electrolyte: 1) $BiVO_4$ (dark), 2) $BiVO_4$-TiO_2 (dark)), 3) $BiVO_4$ (illumination) and 4- $BiVO_4$-TiO_2 (illumination)*

Effect of PEDOT on the EC behavior of $BiVO_4$ thin film

FTO-modified PEDOT occluded with $BiVO_4$ or $BiVO_4$-TiO_2 was subjected to CV studies in the dark and under illumination, the results are shown in Figures 6 and 7. Figure 6 shows that PEDOT increases the photocurrent of $BiVO_4$ during cathode scanning. On the other hand, Figure 7A shows that PEDOT did not increase the $BiVO_4$-TiO_2 photocurrent in the cathode scan (shaded traces 2 and 3). This can be explained if consideration is given to the possibility of the formation of a broken-band alignment between PEDOT and $BiVO_4$-TiO_2 with n-type heterojunction. Figure 7B shows that a larger photocurrent was recorded in the anode scan for $BiVO_4$-TiO_2/PEDOT (trace 3) than for solely $BiVO_4$-TiO_2 (trace 2). The band alignments between PEDOT and $BiVO_4$-TiO_2 (Figure 8) show higher HOMO energy for PEDOT than that of the conduction band of $BiVO_4$-TiO_2. In broken-band alignments, the current transport [39] can be achieved with three mechanisms: 1) interface tunneling, 2) drift-diffusion, and 3) ballistic tunneling. Any of these mechanisms can negatively affect the photocurrent outcome of the assembly. The fact that such behavior was not reported with $BiVO_4$/PEDOT suggests that the presence of TiO_2 as a dopant created a different subband at the interface with PEDOT.

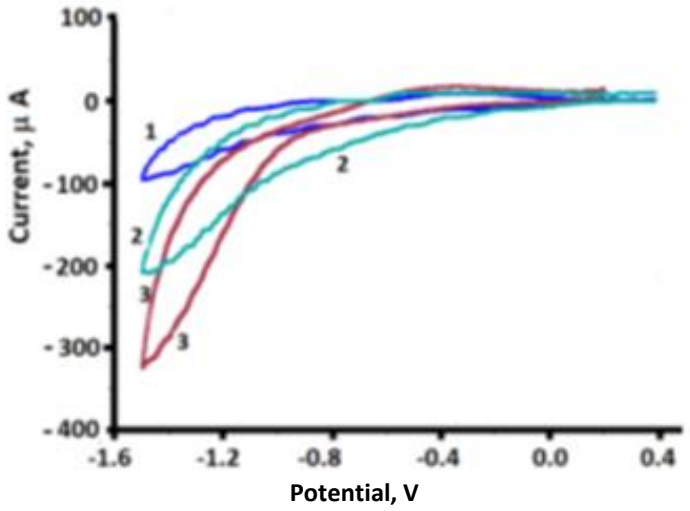

Figure 6. *I/µA and E/V at scan rate 0.1 V s^{-1} for $BiVO_4$/FTO/gel electrolyte: 1) $BiVO_4$ (dark), 2) $BiVO_4$ (illumination), and 3) PEDOT/ $BiVO_4$ (illumination)*

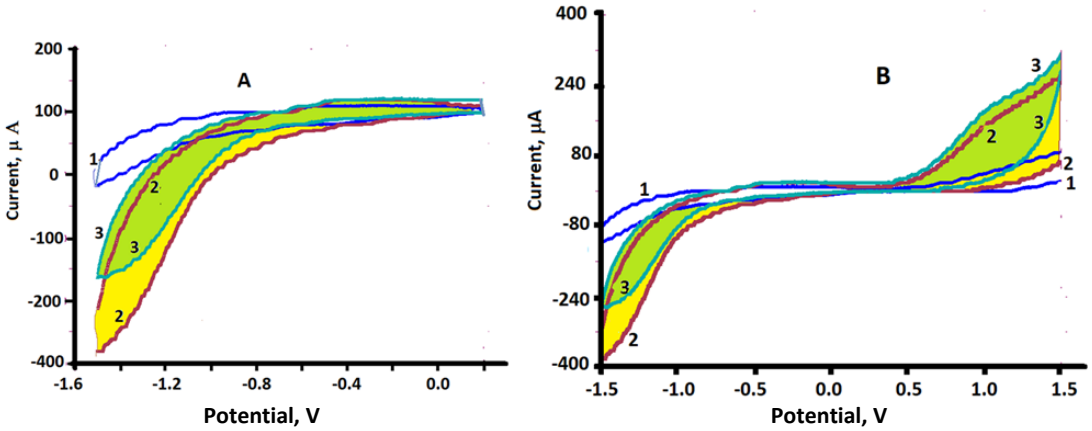

Figure 7. *I/μA and E/V at scan rate 0.1 V s^{-1} for $BiVO_4$-TiO_2/FTO in gel electrolyte: A) cathodic scan, and B) anodic scan for: 1 - $BiVO_4$-TiO_2 (dark), 2 - $BiVO_4$-TiO_2 (illumination), 3 - PEDOT/ $BiVO_4$-TiO_2 (Illumination)*

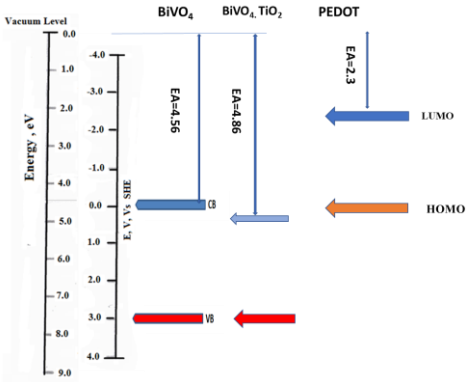

Figure 8. *Band energy map of the studied assemblies*

Chronoamperometric studies

Figure 9 displays the chronoamperometric studies at -1.20 V for FTO/ $BiVO_4$ and FTO/PEDOT--$BiVO_4$ (Figure 9A) and for FTO/$BiVO_4$-TiO_2 and FTO/PEDOT-$BiVO_4$-TiO_2 (Figure 9B). It can be noticed that in all studied assemblies, the gradual increase in photocurrent and the lack of sudden photocurrent rise indicate that the studied interfaces did not generate hole accumulation. On the other hand, under dark conditions, no sudden drop in the measured current instead a gradual drop of the measured current took place for ≈200 s (shaded area). The current generated in the absence of incident light photons is known as dark current, which may reflect the random generation of electrons and holes within the depletion region at the interface [40,41]. Figure 9A and B shows that such behavior is reproducible with less photocurrent generation.

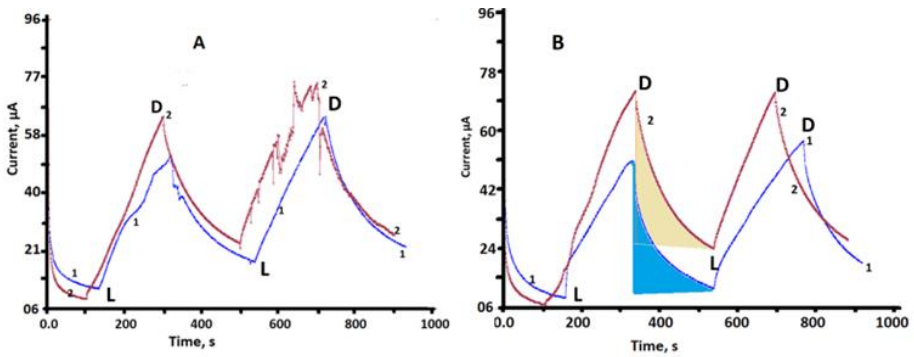

Figure 9. *Chronoamperometric studies at -1.20 V vs. platinized FTO for: A) 1- FTO/$BiVO_4$, 2- FTO/$BiVO_4$/PEDOT, and B) 1- FTO/$BiVO_4$-TiO_2 ,2- FTO/$BiVO_4$-TiO_2/PEDOT(D = dark, L = light)*

Electrochemical impedance spectroscopy

Impedance spectra of the assemblies FTO/$BiVO_4$, FTO/$BiVO_4$-TiO_2, FTO/$BiVO_4$/PEDOT, and FTO/$BiVO_4$-TiO_2/PEDOT were measured between 10^5 and 10^{-2} Hz. Nyquist plot, as well as other dielectric properties generated from the assemblies on FTO substrate in the dark and under illumination, are displayed in Figures 9, 10, 11, and 12.

Effect of TiO_2 doping in $BiVO_4$

Nyquist plots as well as conductivity measurements for FTO/$BiVO_4$ and FTO/$BiVO_4$-TiO_2, are displayed in Figures 10 and 11, respectively. Figure 10 shows both kinetic and diffusional control across the studied frequency range. The figure also shows that illumination increases the resistance (real impedance) and decreases the imaginary component of the studied assembly. This may be attributed to the fact that upon illumination, the photogenerated charges affect the charge transport properties. The generated electron/hole (e/h) pairs change the charge carriers' density, this will lead to a decrease in its mobilities and therefore increases the impedance. The fact that illumination increases the real impedance (true resistance) and decreases the imaginary impedance may reflect fewer effects on the inductive and capacitive impedances but more effects on the resistance. Furthermore, the doping of $BiVO_4$ with TiO_2 results in increases in the impedance. The shape of an un-concentered semicircle at high frequencies and the existence of Warburg impedance reflect the film porosity [42].

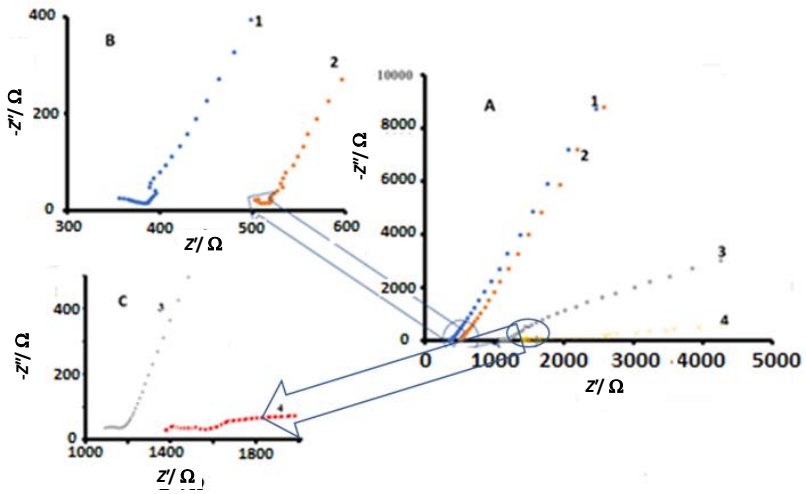

Figure 10. *Nyquist plot at -1.200 V* vs. *platinized FTO for: A) 1 - $BiVO_4$ D, 2 - $BiVO_4$ L , 3 - $BiVO_4$-TiO_2 D, 4 - $BiVO_4$-TiO_2 L , B) and C) are exploded views (D = dark, L = light)*

The dielectric behavior of the generated assemblies was explored at 25 °C, by further treatment of EIS data for each assemblies. The AC conductivity was calculated using the following equation [43]:

$$\sigma_{ac} = \frac{L}{a}\frac{Z'}{Z'^2 + Z''^2} \quad (5)$$

where σ_{ac} is ac conductivity, L is film thickness, m, and a is electrode surface area, m^2. Z' and Z'' are the real and imaginary impedance, respectively. Figure 11 is the plot of the log σ_{ac} *vs*. log ω. This figure clearly shows that under illumination the ac conductivity increases by raising the frequency for FTO/$BiVO_4$ up to 100 Hz (Figure 11, trace 1, 2) after which the conductivity becomes independent of frequency. However, the illuminated $BiVO_4$ shows less conductivity than that measured in the dark. Similar behavior was reported with FTO/$BiVO_4$-TiO_2 (Figure 10, trace 3, 4) showing that, in the dark, the conductivity of $BiVO_4$-TiO_2 increases by raising the frequency to 100 Hz. However, under

illumination, the conductivity continues to increase by increasing frequency up to 10 kHz (Figure 11, trace 4). Figure 11 shows that the addition of TiO_2 to $BiVO_4$ causes a decrease in the AC conductivity in comparison to that of $BiVO_4$. This decrease in conductivity may be attributed to the increase in the capacitive reactance of the assembly. This leads to an increase in the impedance and consequently decreases the AC conductivity. The conductivity can also increase due to the hopping of charge carriers at high frequencies.

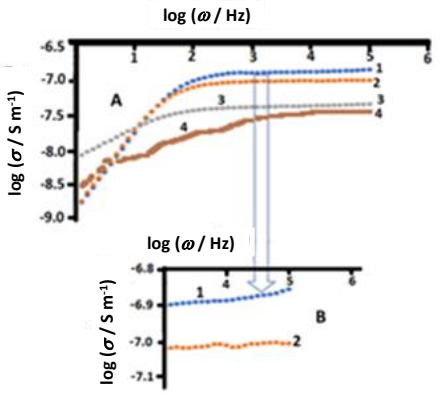

Figure 11. *A) log* σ vs. *log* ω*, of the 1- $BiVO_4$ D, 2- $BiVO_4$ L, 3- $BiVO_4$-TiO_2 D, and 4- $BiVO_4$-TiO_2 L; B) exploded view (D=Dark, L =Light)*

Similar results were obtained when FTO/$BiVO_4$ was interfaced with PEDOT (Figures 12 and 13). Figure 12A (trace 1, 2) shows that interfacing $BiVO_4$-TiO_2 with PEDOT results in similar results to that without PEDOT (Figure 10 A, trace 1, 2), where the illuminated interface shows increasing both real and imaginary impedance of the assembly. The doping of $BiVO_4$ with TiO_2 and interfacing it with PEDOT alters the equivalent circuits of this interface to include more inductive and capacitive elements (Figure 12 A, trace 3, 4).

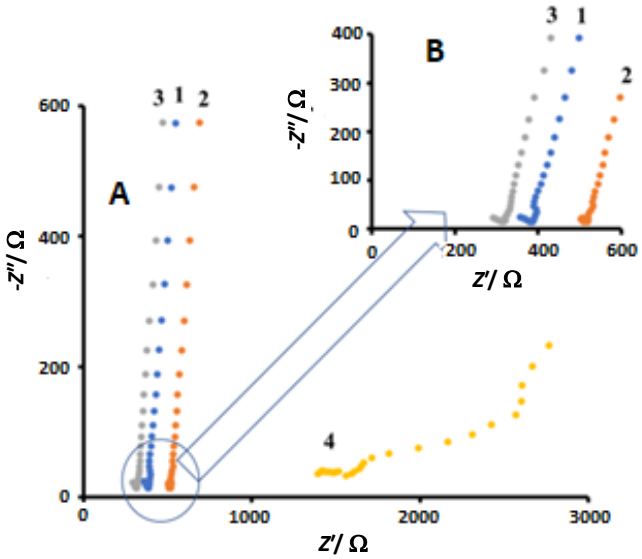

Figure 12. *Nyquist plots at -1.20 V* vs. *platinized FTO for the assemblies FTO/$BiVO_4$/PEDOT, and FTO/$BiVO_4$-TiO_2/PEDOT: A) 1- $BiVO_4$/PEDOT D, 2- $BiVO_4$/PEDOT L, 3- $BiVO_4$-TiO_2/PEDOT D, 4- $BiVO_4$-TiO_2/PEDOT L, B) exploded view. (D = dark, L = light)*

Figure 13 is the plot of the log of conductivity *vs*. log frequency. Under illumination, the AC conductivity increases by raising the frequency for studied assemblies to ≈300 Hz (Figure 13, traces 1,2,3, and 4) after which the conductivity becomes independent of frequency. However, illumination

decreases the AC conductivity, especially at frequencies greater than 100 Hz. Such behavior can be attributed to the decrease in conductivity due to the increase in the capacitive reactance of the assembly.

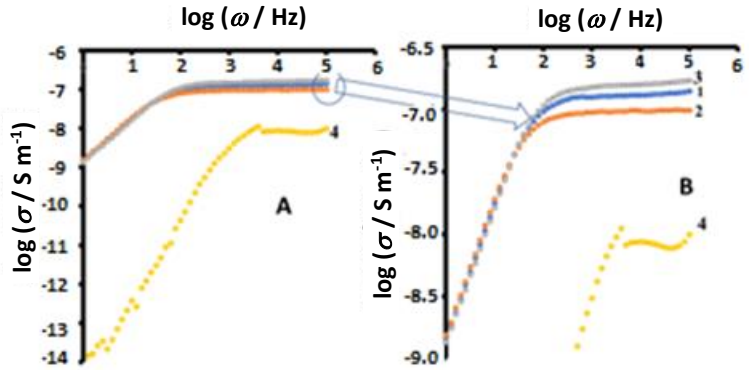

Figure 13. *Log electrical conductivity vs. log frequency of the 1 - $BiVO_4$ /PEDOT D, 2 - $BiVO_4$ /PEDOT L, 3 - $BiVO_4$-TiO_2/PEDOT D, and 4 - $BiVO_4$-TiO_2/PEDOT L: A) log conductivity σ vs. log frequency, B) exploded view. (D = dark, L = light)*

Conclusion

Photoelectrochemical behavior (PEC) of mixed transition and post-transition metal oxides with or without interfacing with PEDOT in thermoplastic gel electrolyte (TPGE) shows that gel electrolyte has proven validity in electrochemical measurements. In comparison with the studies took place in liquid or aqueous electrolytes, the results obtained in gel electrolytes were reproducible and consistent. This confirms our assumption of the validity of gel electrolytes in electrochemical studies with mixed metal oxide systems. The noticeable photoactivity outcome confirms that mixed-metal oxide composites are excellent photocatalysts even in gel electrolytes. The results obtained in this study will add to the data bank of electrochemical studies in gel electrolytes.

Declaration of competing interest: *The authors declare that they have no known competing financial interests or personal relationships that could have appeared to influence the work reported in this paper.*

Acknowledgment: *The authors acknowledge the support for this work from Indiana University Kokomo.*

References

[1] M. L. Grilli, Metal Oxides, *Metals* **10** (2020) 820. https://doi.org/10.3390/met10060820

[2] D. Nunes, A. Pimental, L. Santos, P. Barquinha, L. Pereira, E. Fortunato, R. Martins, *Metal Oxide Nanostructures: synthesis, properties and applications,* Elsevier, 2019, 59-102. https://doi.org/10.1016/C2016-0-01647-9

[3] M. L. Grilli, L. Chevallier, M. L. Di Vona, S. Licoccia, E. Di Bartolomeo. Planar electrochemical sensors based on YSZ with WO_3 electrode prepared with different chemical routes, *Sensors and Auctuators B* **111-112** (2005) 91-95. https://doi.org/10.1016/j.snb.2005.06.035

[4] M. L. Grilli, N. Kaabbuathong, A. Dutta, E. Di Bartolomeo, E Traversa, Electrochemical NO_2 sensors with WO_3 electrodes for high temperature applications, *Journal of the Ceramic Society of Japan* **110** (2002) 159-162. https://doi.org/10.2109/jcersj.110.159

[5] S. Aydoğan, M.L Grilli, M. Yilmaz, Z. Çaldiran, H. Kaçuş, A facile growth of spray based ZnO films and device performance investigation for Schottky diodes: Determination of interface state density distribution, *Journal of Alloys and Compounds* **708** (2017) 55-66. http://dx.doi.org/10.1016/j.jallcom.2017.02.198

[6] M. Yilmaz, M. L. Grilli, G. A. Turgut, A Bibliometric Analysis of the Publications on In Doped ZnO to be a Guide for Future Studies, *Metals* **10** (2020) 598. https://doi.org/10.3390/met10050598

[7] S. Glass, B. Trinklein, B. Abel, A. Schulze, TiO_2 as photosensitizer and photoinitiator for synthesis of photoactive TiO_2-PEGDA hydrogel without organic photoinitiator, *Frontiers in Chemistry* **6** (2018) 340. https://doi.org/10.3389/fchem.2018.00340

[8] J. Sun, W. Xia, Q. Zheng, X. Zeng, W. Liu, G. Liu, P. Wang. Increased active sites on irregular morphological α-Fe_2O_3 nanorods for enhanced photoelectrochemical performance, *ACS Omega* **5(21**) (2020) 12339-12345. https://doi.org/10.1021/acsomega.0c01072

[9] S. N. F. Moridon, M. N.I. Salehmin, K. Arifin, L.J. Minggu, M.B. Kassim, Synthesis of cobalt oxide on FTO by hydrothermal method for photoelectrochemical water splitting application. *Applied Sciences* **11(7)** (2021) 3031. https://doi.org/10.3390/app11073031

[10] M. Wang, J. Han, R.Guo, H. Xiong, Y. Yin, TiO_2/NiO hybrid shells: p-n junction photocatalysts with enhanced activity under visible light, *Journal of Materials Chemistry A* **3** (2015) 20727-20735. https://doi.org/10.1039/C5TA05839B

[11] W. Zhou, H. Liu, J. Wang, D. Liu, G. Du, J. Cui, Ag_2O/TiO_2 nanobelts heterostructure with enhanced ultraviolet and visible photocatalytic activity, *ACS Applied Materials & Interfaces* **2** (2010) 2385-2392. https://doi.org/10.1021/am100394x

[12] S. Sood, S.K. Mehta, A.S.K. Sinha, S.K. Kansal, Bi_2O_3/TiO_2 heterostructures: synthesis, characterization and their application in solar light mediated photocatalyzed degradation of an antibiotic, ofloxacin, *Chemical Engineering Journal* **290** (2016) 45-52. https://doi.org/10.1016/j.cej.2016.01.017

[13] D. Ramírez-Ortega, P. Acevedo-Peña, F. Tzompantzi, R. Arroyo, F. González, I. González, Energetic states in SnO_2-TiO_2 structures and their impact on interfacial charge transfer process, *Journal of Materials Science* **52** (2017) 260-275. https://doi.org/10.1007/s10853-016-0328-3

[14] L. Ren, W. Zhou, B. Sun, H. Li, P. Qiao, Y. Xu, J. Wu, K. Lin, H. Fu, Defects-engineering of magnetic γ-Fe_2O_3 ultrathin nanosheets/mesoporous black TiO_2 hollow sphere heterojunctions for efficient charge separation and the solar-driven photocatalytic mechanism of tetracycline degradation, *Applied Catalysis B* **240** (2019) 310-319. https://doi.org/10.1016/j.apcatb.2018.08.033

[15] V. Neburchilov, H. Wang, J. J. Martin, W. Qu, A review on air cathodes for zinc-air fuel cells, *Journal of Power Sources* **195** (2010) 1271-1291. https://doi.org/10.1016/j.jpowsour.2009.08.100

[16] L. Kong, H. Chen, W. Hua, S. Zhang, J. Chen, Mesoporous bismuth titanate with visible-light photocatalytic activity, *Chemical Communications* **77** (2008) 4977-4979. https://doi.org/10.1039/B808911F

[17] Y. Hosogi, Y. Shimodaira, H. Kato, H. Kobayashi, A. Kudo, Role of Sn^{2+} in the Band Structure of SnM_2O_6 and $Sn_2M_2O_7$(M = Nb and Ta) and Their Photocatalytic Properties, *Chemistry of Materials* **20(4)** (2008) 1299-1307. https://doi.org/10.1021/cm071588c

[18] A. Walsh, Y. Yan, M.N. Huda, M.M. Al-Jassim, S.-H. Wei, Band Edge Electronic Structure of $BiVO_4$: Elucidating the Role of the Bi s and V d Orbitals, *Chemistry of Materials* **21** (2009) 547-551. https://doi.org/10.1021/cm802894z

[19] Y. Hu, W. Chen, J. Fu, M. Ba, F. Sun, P. Zhang, J. Zou, Hydrothermal synthesis of $BiVO_4$/TiO_2 composites and their application for degradation of gaseous benzene under visible light irradiation, *Applied Surface Science* **436** (2018) 319-326. https://doi.org/10.1016/j.apsusc.2017.12.054

[20] F. F. Abdi, R. van de Krol, Nature and Light Dependence of Bulk Recombination in Co-Pi-Catalyzed $BiVO_4$ Photoanodes, *Journal of Physical Chemistry C* **116** (2012) 9398-9404. https://doi.org/10.1021/jp3007552
[21] K. Zhang, X.-J. Shi, J.K. Kim, J.H. Park, Photoelectrochemical Cells with Tungsten Trioxide/Mo-Doped BiVO4 Bilayers, *Physical Chemistry Chemical Physics* **14** (2012) 11119-11124. https://doi.org/10.1039/C2CP40991G
[22] F. F. Abdi, T. J. Savenije, M. M. May, B. Dam, R. van de Krol, The Origin of Slow Carrier Transport in $BiVO_4$ Thin Film Photoanodes: A Time-Resolved Microwave Conductivity Study, *The Journal of Physical Chemistry Letters* **4** (2013) 2752−2757. https://doi.org/10.1021/jz4013257
[23] M. S. Tamboli, H. S. Jadhav, D. R. Patil, A. F. Shaikh, S. S. Patil, J. G. Seo, H. Choi, S. W. Gosavi, B.B. Kale, Hierarchical novel $NiCo_2O_4$/$BiVO_4$ hybrid heterostructure as an advanced anode material for rechargeable lithium ion battery, *International Journal of Energy Research* **44** (2020) 12126-12135. https://doi.org/10.1002/er.5755
[24] L. Hu, X. Chen, C. Feng, Synthesis and electrochemical performances of $BiVO_4$/CNTs composite as anode material for lithium-ion battery, *Ionics* **28** (2022)1483-1493. https://doi.org/10.1007/s11581-022-04456-z
[25] Z. Lei, N. Christov, X.S. Zhao, Intercalation of mesoporous carbon spheres between reduced graphene oxide sheets for preparing high-rate supercapacitor electrodes, *Energy and Environmental Science* **4** (2011) 1866-1873. https://doi.org/10.1039/C1EE01094H
[26] Z. Chen, Y. Qin, D. Weng, Q. Xiao, Y. Peng, X. Wang, H. Li, F. Wei, Y. Lu, Design and Synthesis of Hierarchical Nanowire Composites for Electrochemical Energy Storage, *Advanced Functional Materials* **19** (2009) 3420-3426. https://doi.org/10.1002/adfm.200900971
[27] X. Dong, Y. Cao, J. Wang, M.B. Chan-Park, L. Wang, W. Huang, P. Chen, Hybrid structure of zinc oxide nanorods and three dimensional graphene foam for supercapacitor and electrochemical sensor applications, *RSC Advances* **2** (2012) 4364-4369. https://doi.org/10.1039/C2RA01295B
[28] H.-L. Hsu, C.-F. Tien, Y.-T. Yang, J. Leu, Dye-sensitized solar cells based on agarose gel electrolytes using allylimidazolium iodides and environmentally benign solvents, *Electrochimica Acta* **91** (2013) 208-213. https://doi.org/10.1016/j.electacta.2012.12.133
[29] J. Tauc, Optical properties and electronic structure of amorphous Ge and Si, *Materials Research Bulletin* **3** (1968) 37-46. https://doi.org/10.1016/0025-5408(68)90023-8
[30] M. Mobin, R. Aslam, J. Aslam, Synergistic effect of cationic gemini surfactants and butanol on the corrosion inhibition performance of mild steel in acid solution, *Materials Chemistry and Physics* **223** (2019) 623-633.https://doi.org/10.1016/j.matchemphys.2018.11.032
[31] N. M. Ravindra, P. Garapathy, J. Choi, Energy gap-refractive index relations in semiconductors: An overview, *Infrared Physics & Technology* **50** (2007) 21-29. https://doi.org/10.1016/j.infrared.2006.04.001
[32] T. S. Moss, *Photoconductivity in the elements,* Academic Press Inc. New York, 1952. https://www.worldcat.org/title/1820280?oclcNum=1820280
[33] T. S. Moss, Relations between the Refractive Index and Energy Gap of Semiconductors, *Physica Status Solidi B* **131** (1985) 415-427. https://doi.org/10.1002/pssb.2221310202
[34] S. Bakhtiarnia, S. Sheibani, A. Billard, E. Aubry, M. Arab Pour Yazdi, Deposition of nanoporous $BiVO_4$ thin-film photocatalyst by reactive magnetron sputtering: Effect of total pressure and substrate, *Transactions of Nonferrous Metals Society of China* **32(3)** (2022) 957-971. https://doi.org/10.1016/S1003-6326(22)65846-1
[35] P. Sharma, S.C. Katyal, Effect of Cd and Pb impurities on the optical properties of fresh evaporated amorphous $(As_2Se_3)_{90}Ge_{10}$ thin films, *Journal of Physics D* **40(7)** (2007) 2115. https://doi.org/10.1088/0022-3727/40/7/038

[36] T. C. Sabari Girisun, S. Dhanushkodi, Linear and nonlinear optical properties of tris thiourea zinc sulphate single crystals, *Crystal Research & Technology* **44(12)** (2009) 1297-1302. https://doi.org/10.1002/crat.200900351

[37] J. T. Edwards, D. J. Thouless, Numerical studies of localization in disordered systems**,** *Journal of Physics C: Solid State Physics* **5** (1972) 807. https://doi.org/10.1088/0022-3719/5/8/007

[38] P. Drude, Zur Elecktronentheorie der Metalle*, Annalen der Physik* **306** (1900) 566-613. https://doi.org/10.1002/andp.19003060312

[39] S.H. Song, E.S. Aydil, S.A. Campbell, Metal-oxide broken-gap tunnel junction for copper indium gallium diselenide tandem solar cells, *Solar Energy Materials and Solar Cells* **133** (2015) 133-142. http://dx.doi.org/10.1016/j.solmat.2014.10.046

[40] E. Go, H. Jin, S. Yoon, S. Park, S.H. Park, H. Yu, H.J. Son, Unraveling the Origin of Dark Current in Organic Bulk Heterojunction Photodiodes for Achieving High Near-Infrared Detectivity, *ACS Photonics* **9(6)** (2022) 2056-2065. https://doi.org/10.1021/acsphotonics.2c00193

[41] C. Li, Y. Bando, M. Liao, Y. Koide, D. Golberg, Visible-blind deep-ultraviolet Schottky photodetector with a photocurrent gain based on individual Zn_2GeO_4 nanowire*, Applied Physics Letters* **97** (2010) 161102. https://doi.org/10.1063/1.3491212

[42] H. Kaiser K. D. Beccu, M. A. Gutjahr*,* Abschätzung der porenstruktur poröser elektroden aus impedanzmessungen, *Electrochimica Acta* **21** (1976) 539-543. https://doi.org/10.1016/0013-4686(76)85147-X

[43] J. H. Joshi, D. K. Kanchan, J. M. Joshi, H. O. Jethva, K. D. Parikh, Dielectric relaxation, complex impedance and modulus spectroscopic studies of mix phase rod like cobalt sulfide nanoparticles*, Materials Research Bulletin* **93** (2017) 63-73. https://doi.org/10.1016/j.materresbull.2017.04.013